Electrochimica Acta 574 (2026) 149566

Contents lists available at ScienceDirect

Electrochimica Acta

journal homepage: www.journals.elsevier.com/electrochimica-acta

Quantification and deconvolution of gas diffusion and conversion losses in solid oxide single-cell testing

D. Esau *, D. Ewald, C. Grosselindemann, A. Weber

Institute for Applied Materials – Electrochemical Technologies (IAM-ET), Karlsruhe Institute of Technology (KIT), Adenauerring 20b, Karlsruhe, D-76131, Germany

ARTICLE INFO

Keywords:
Solid oxide cell testing
Gas diffusion
Gas conversion
Ni/YSZ
Ni/GDC

ABSTRACT

Concentration-related changes of the Nernstian voltage inevitably contribute to the resistance observed during DC operation of solid oxide cells. In electrochemical impedance spectroscopy (EIS), concentration losses arising from gas diffusion and gas conversion often overlap with electrochemical polarization processes, which is particularly true for high-capacitance mixed-ionic–electronic conducting electrodes, complicating the interpretation of impedance spectra and extracted activation energies. This work presents a comprehensive in-operando methodology to deconvolute gas diffusion and gas conversion resistances in electrolyte supported cells with screenprinted electrodes. Gas diffusion losses are quantified using an extended inert-diluent variation approach, enabling the determination of an effective microstructure parameter and prediction of diffusion resistances at arbitrary operating conditions. An alternative method based on replacing hydrogen/steam with carbon monoxide/carbon dioxide is introduced to access the same parameter, applicable to electrodes exhibiting a separable low-frequency concentration feature, such as nickel / yttria stabilized zirconia (Ni/YSZ). Furthermore, a novel approach for determining gas conversion resistances is presented, avoiding reliance on idealized analytical models, and enabling accurate prediction of concentration losses over a wide range of gas compositions and temperatures. The combined prediction of diffusion and conversion losses accurately reproduces the total concentration impedance over a broad steam partial pressure range and outperforms existing analytical approaches. The methodology is demonstrated on a commercial full cell, containing a nickel / gadolinia-doped ceria (Ni/GDC) fuel electrode, allowing reliable extraction of intrinsic activation energies even in the presence of increased, setup-induced concentration losses.

1. Introduction

The ongoing commercialization of solid oxide electrolyzers underscores the growing need for reliable testing of materials under technically relevant operating conditions. Often employed are single-cell tests with reduced active area (<1–16 cm^2), compared to stack cells (often > 100 cm^2). Scaling the geometrical electrode area down to 1 cm^2 combined with elevated flow rates to minimize gas conversion effects, gradients along the cell length are minimized. This offers a unique opportunity for extracting material specific relations between operation conditions (temperature, concentration) and cell resistance, which are quantifiable by kinetic approaches and their parameter sets. Such parameter sets include e.g. exchange current densities of electrochemical reactions and their activation energies which implicitly contain information about the present reaction mechanisms [1,2].

However, in solid oxide cells, a variety of loss processes occur simultaneously and are highly convoluted if only the DC operation state is analyzed. Deconvoluting these processes enables identification of dominant performance-limiting and degradation-related contributions across different operating conditions and provides a basis for targeted mitigation strategies. Electrochemical impedance spectroscopy (EIS), ideally combined with the subsequent distribution of relaxation times (DRT) analysis offers a frequently applied possibility for the deconvolution of loss processes, as long as the processes are sufficiently separated by a difference in time constants. Challenges arise, if multiple processes occur at similar relaxation frequencies and thus overlap in the measured impedance spectra and DRT. If anode and cathode responses overlap, symmetrical cells can be employed [3] or one electrode can be substituted by a material with a larger or smaller time constant in order to isolate the electrode response of interest [4]. When isolated, a single porous electrode response contains loss contributions from charge transport, the electrochemical reaction(s) with all contributing reaction steps and concentration differences affecting the Nernst potential. These

* Corresponding author.
E-mail address: daniel.esau@kit.edu (D. Esau).

https://doi.org/10.1016/j.electacta.2026.149566
Received 13 May 2026; Received in revised form 14 July 2026; Accepted 15 July 2026
Available online 17 July 2026
0013-4686/© 2026 The Authors. Published by Elsevier Ltd. This is an open access article under the CC BY license (http://creativecommons.org/licenses/by/4.0/).

Nomenclature

Abbreviations

3YSZ	3 mol% yttria-stabilized zirconia
CNLS	Complex-nonlinear least squares
CO	Carbon monoxide
CO_2	Carbon dioxide
CSTR	Continuously-stirred-tank reactor
DRT	Distribution of relaxation times
EIS	Electrochemical impedance spectroscopy
ESC	Electrolyte supported cell
FESC	Fuel electrode supported cell
GDC	Gadolinia-doped ceria
H_2O	Steam
H_2	Hydrogen
He	Helium
LSCF	Lanthanum-strontium-cobalt-ferrite
MIEC	Mixed-ionic-electronic conductor
N_2	Nitrogen
O_2	Oxygen
OCV	Open circuit voltage
PFR	Plug-flow reactor
SO(F/E)C	Solid oxide (fuel / electrolyzer) cell

Symbols

C	Constant (var.)
D	Diffusion coefficient ($m^2\ s^{-1}$)
F	Faraday constant (96,485 A s mol^{-1})
G	Microstructure parameter (m^{-1})
J	Molar flow rate per cell area (mol $cm^{-2}\ s^{-1}$)
L	Diffusion length (m)
Λ	Effective gas diffusion or gas conversion term (var.)
P	Pressure (atm)
Ψ	Microstructure parameter (-)
R	Area specific resistance ($\Omega\ cm^2$)
$\widetilde{R}$	Universal gas constant, (8.314 J $mol^{-1}\ K^{-1}$)
T	Temperature (K)
x	Molar fraction (-)

Sub- and superscripts

AE	air electrode
calib	calibrated
conv	conversion
diff	diffusion
eff	effective
HF	high-frequency
in	inlet
LF	low-frequency
MC	multi-component
meas	measured
Pol	Polarization

contributions again, can appear as overlapping processes and then require deconvolution via modeling approaches.

Electrodes which contain fluorite or perovskite mixed-ionic-electronic conducting (MIEC) materials with high chemical capacitances, originating from the variation of non-stoichiometric oxygen content in the material, may eventually show a single undifferentiable impedance response associated with the concentration impedance in superposition with the electrochemical response of the porous electrode (reaction coupled with charge transport) [3–8]. When the electrode performance is high, the resulting Arrhenius plot of the fitted resistance does not appear as a straight line but flattens towards higher temperatures due to the weak temperature dependency of concentration losses [9,10].

Nenning et al. performed a correction by direct fitting of the gas diffusion resistance from the Arrhenius graph to obtain the intrinsic activation energy of the electrode [9]. However, the direct fit to a modified Arrhenius equation might yield resistance values which are not unique, so a good estimate of the diffusion resistance is required.

Riegraf et al. used a concentration resistance value, that was taken from previous investigations performed on nickel/yttria stabilized zirconia (Ni/YSZ) electrodes in exactly the same test bench, to correct the measured activation energy [10]. The weak temperature dependence of the concentration resistance was modelled based on an explicit equation for the gas diffusion resistance, first derived by Primdahl and Mogensen [11]:

$$R_{\mathrm{Diff}} = \left(\frac{\widetilde{R}T}{2F}\right)^2 \frac{L}{\Psi}\left(\frac{1}{D_{\mathrm{H_2O}} x_{\mathrm{H_2O}}} + \frac{1}{D_{\mathrm{H_2}} x_{\mathrm{H_2}}}\right)\frac{1}{P}, \tag{1}$$

with $\widetilde{R}$ as the gas constant, F the Faraday constant, L the gas diffusion layer thickness, Ψ the microstructure parameter within the gas diffusion layer, P the pressure, D the molecular diffusion coefficient, and $x_{\mathrm{H_2}}$ / $x_{\mathrm{H_2O}}$ the molar fraction of hydrogen / steam. If only molecular diffusion in the flow channel geometry, current collector and, in case of fuel electrode supported cells, the supporting substrate are considered and the gas diffusion within a thin, sufficiently porous active electrode layer can be neglected, the method gives acceptable results. Nevertheless, the method requires *a-priori* knowledge of a concentration resistance in an identical setup.

Furthermore, the gas diffusion resistance can be derived from measurements with ternary gas mixtures of hydrogen (H_2), steam (H_2O) and two different inert diluents (Nitrogen and Helium) [3]. From the difference in polarization resistance between the measurement in Helium and Nitrogen, an effective microstructure parameter

$$G_{\mathrm{eff}} = \frac{\Psi}{L} \tag{2}$$

can be derived:

$$G_{\mathrm{eff}} = \left(\frac{\widetilde{R}T}{2F}\right)^2 \frac{1}{R_{\mathrm{pol,N_2}} - R_{\mathrm{pol,He}}} \cdot \ldots$$

$$\left(\frac{1}{D_{\mathrm{H_2O,(H_2,N_2)}} x_{\mathrm{H_2O}}} + \frac{1}{D_{\mathrm{H_2,(H_2O,N_2)}} x_{\mathrm{H_2}}} - \frac{1}{D_{\mathrm{H_2O,(H_2,He)}} x_{\mathrm{H_2O}}} - \frac{1}{D_{\mathrm{H_2,(H_2O,He)}} x_{\mathrm{H_2}}}\right)\frac{1}{P}, \tag{3}$$

and used to model the gas diffusion resistance at arbitrary concentration and temperature, applying the equation by Primdahl and Mogensen [11]. In that way, gas diffusion contributions can be directly obtained *in operando* and no previous measurement or estimation is required.

Gas conversion resistances on the other hand, are rarely considered explicitly. They arise due to in-plane concentration differences between inlet and electrode surface in a situation where *convective* gas transport in the channel is determining the loss mechanism, affecting the Nernst potential [12]. Conversion resistances are thus solely a result of the measurement setup and not of the tested cell. They depend on gas flow rate, gas composition, cell area and current density. Close to the open circuit voltage (OCV), and under the premise of small relative concentration changes between inlet and outlet, the resistance can be linearized. Primdahl and Mogensen were the first to present an equation that predicts the (small signal, e.g. for EIS) gas conversion resistance [13]. They derived the following expression to predict the gas conversion

resistance R_{conv}^{CSTR} arising from the volume above the fuel electrode in a continuously-stirred-tank reactor (CSTR) setup:

$$R_{Conv}^{CSTR} = \frac{\widetilde{R}T}{4F^2 J_{in}} \left(\frac{1}{x_{in,H_2O}} + \frac{1}{x_{in,H_2}} \right), \quad (4)$$

where J_{in} denotes the molar flow rate per geometric electrode area (mol cm^{-2} s^{-1}). Later, Jensen et al. modified the equation for a plug-flow-reactor (PFR) setup [14]. In their derivation they account for the fact that in a long channel, concentration above the electrode does not change equally along the channel coordinate (CSTR assumption) but rather is a function of the channel coordinate (PFR assumption). The result is a difference in factor of 2 between the CSTR and the PFR case:

$$R_{conv}^{PFR} = \frac{\widetilde{R}T}{8F^2 J_{in}} \left(\frac{1}{x_{in,H2O}} + \frac{1}{x_{in,H_2}} \right). \quad (5)$$

Ebbesen et al. have analyzed the low-frequency resistance contribution of 16 cm^2 fuel electrode supported cells (FESC) with Ni/YSZ fuel electrodes [15]. At open circuit voltage they observed that the "low--frequency concentration related resistance", lies between the prediction of the PFR-model and the CSTR-model. However, they confirmed that the concentration resistance follows the trends predicted by Eq. (4) and (5), such as: 1) a linear dependency on the inverse flow rate and 2) the expected concentration dependency. Also, in the study by Njodzefon et al. the fitted gas conversion resistance of a 16 cm^2 Ni/YSZ FESC lied between the predictions of PFR- and CSTR-model [16]. In the case of a 4 × 0.5 cm (length x width) electrode, the conversion resistance was even better described by the CSTR model, despite the long cell geometry would rather implicate that the PFR model should be applied.

This raises the question whether idealized equations such as Eq. (4) and (5) can be straightforwardly used to predict the gas conversion resistance in a real testing setup. Especially, in the case of the earlier discussed MIECs with large chemical capacitances, diffusion and conversion resistances must be accurately predicted and deconvoluted from the electrochemical porous electrode response to extract meaningful kinetic parameters of the electrochemical surface reaction. Thus, this study aims to offer novel experimental designs to determine the gas diffusion and gas conversion resistances of single cells *in operando*.

The methods are exemplified and validated on a symmetrical cell with Ni/YSZ electrodes and a commercial electrolyte supported full cell containing a Nickel / gadolinia doped ceria (Ni/GDC) fuel electrode. We show, that with the help of the presented methods, the total concentration resistance (i.e. the sum of gas diffusion and gas conversion resistance) can be accurately predicted in a wide steam partial pressure range. Hereby, the novel method for determining and predicting the gas conversion resistance outperforms previous analytical approaches [13, 14]. In the case of the Ni/GDC fuel electrode, the methods are used to show the influence of an erroneous experimental setup containing a bypass and how the methods can be applied to correct the influence of the setup and extract the intrinsic activation energy of the thermally activated cell-specific losses.

2. Experimental

Planar cells with an active area of 1 cm^2 were analyzed in this study. Cells with Ni/GDC fuel electrodes were fabricated by Sunfire SE. When full cells were employed, the air electrode was based on GDC/LSCF. The electrodes were printed on a 3 mol% yttria-stabilized zirconia (3YSZ) electrolyte, which was supplied by Kerafol GmbH & Co. KG within the scope of the German H2Giga project. Symmetrical cells with Ni/YSZ electrodes were fabricated in-house; information on this cell type can be found in the work of Sonn et al. [17]. The full cell used for the air electrode analysis in the Appendix was supplied by Elcogen within the scope of the EU Project FlyECO. Standardized reduction procedures were always performed during the startup of each cell, and for reused cells, heating was carried out in a reducing atmosphere.

Electrochemical measurements were conducted using a two-electrode setup in a test rig described in [18]. To generate well-defined H_2/H_2O mixtures, synthetic steam was produced in an upstream combustion chamber by mixing appropriate amounts of oxygen with the fuel. In the case of $H_2/H_2O/CO/CO_2$ mixtures, CO_2 and CO were added downstream of the combustion chamber to avoid unwanted equilibration in the combustion chamber. To ensure a well-defined gas composition at the electrode surface and prevent changes via the (reverse) water-gas shift reaction, the gas mixtures were supplied in an equilibrated state considering the operating temperature of the cell. Equilibrium partial pressure calculations were performed using the software package *Cantera*. Thermodynamic carbon formation was also excluded for every analyzed operating point.

Impedance spectra were acquired using a Solartron 1260 frequency response analyzer (symmetrical cells) or a Zahner ZENNIUM PRO potentiostat (full cells), applying a pseudo-potentiostatic measurement technique. To maintain linear response conditions, a current amplitude resulting in a voltage drop of $\leq$ 12 mV relative to the polarization resistance was selected. Changes in the gas conversion resistance due to different current amplitudes were excluded by calculating the large-signal behavior of the gas conversion overpotential for all measurement conditions, according to Primdahl and Mogensen for the CSTR case [13] and according to Jensen et al. for the PFR case [14], which confirmed that a linear approximation in the current excitation range is valid.

Each measurement was performed over a frequency range from 30 mHz to 1 MHz with 6 points per decade for frequencies larger than 66 Hz and 12 points per decade for frequencies smaller than 66 Hz. Impedance data quality was verified by a Kramers–Kronig test [19]. Fitting of the EIS data and DRT calculation was performed using in-house software.

3. Results and discussion

3.1. Determination of the effective microstructure parameter G_{eff}

Grosselindemann et al. presented a convenient method for *in-operando* quantification of fuel electrode gas diffusion resistance for an electrolyte supported cell [3]. The method requires two EIS measurements performed with identical concentration of the electroactive species (e.g. steam and hydrogen) and two different inert diluents. The concentration of the electroactive species should be low (e.g. 5% steam + 10% hydrogen) and the inert diluents should yield sufficiently different diffusion coefficients of the electroactive species in the inert diluent. A satisfying difference in diffusion coefficients can be obtained by choosing helium vs. nitrogen or helium vs. argon. The effective microstructure parameter G_{eff} can then be obtained from the difference in polarization resistance and with knowledge of the ternary diffusion coefficients, according to Eq. (3). Binary diffusion coefficients were calculated using Chapman–Enskog theory [20,21], from which multi-component diffusion coefficients were obtained using the Wilke formulation [22].

3.1.1. Accessing G_{eff} via a quaternary variation by balancing inert diluents

The method of Grosselindemann et al. calculates the microstructure parameter from only two measurements. To decrease the risk of a single statistical outlier distorting the determination of the microstructure parameter, this method can be extended by performing a quaternary variation with multiple measurements, instead of two measurements with a ternary variation. Now, the ratio of the two inert diluents will be changed successively. The effective microstructure parameter G_{eff} can then be determined from a linear correlation as follows: The original equation by Primdahl and Mogensen [11] tells us that the gas diffusion resistance is linearly correlated with the inverse of G_{eff}:

$$R_{\text{diff}} = G_{\text{eff}}^{-1} \cdot \left(\frac{\widetilde{RT}}{2F}\right)^2 \left(\frac{1}{D_{\text{H}_2\text{O}}^{\text{MC}} x_{\text{H}_2\text{O}}} + \frac{1}{D_{\text{H}_2}^{\text{MC}} x_{\text{H}_2}}\right) \frac{1}{P}, \tag{6}$$

with the multicomponent diffusivities D_{i}^{MC}. Note, that the gas diffusion resistance approaches infinity for mixtures containing either only hydrogen or steam as electroactive compound. EIS measurements under OCV in pure hydrogen therefore usually show high resistances and lack interpretability.

When solely the ratio of the inert diluents is changed the total polarization resistance can be described by:

$$R_{\text{Pol}} = G_{\text{eff}}^{-1} \cdot \underbrace{\left[\left(\frac{\widetilde{RT}}{2F}\right)^2 \left(\frac{1}{D_{\text{H}_2\text{O}}^{\text{MC}} x_{\text{H}_2\text{O}}} + \frac{1}{D_{\text{H}_2}^{\text{MC}} x_{\text{H}_2}}\right) \frac{1}{P}\right]}_{\Lambda_{\text{diff}}} + C_1, \tag{7}$$

where C_1 is the sum of the gas conversion resistance and all thermally activated polarization resistance contributions, which both are never affected by the change of inert diluent. Λ_{diff} is the effective gas diffusion term with the unit resistance times length ($\Omega \cdot$ cm) which is varied when the ratio of the inert diluents is adjusted. G_{eff} is then obtained through a linear fit of Λ_{diff} vs. R_{pol}.

In Fig. 1 the EIS results from a quaternary variation on two different electrolyte supported cells are shown. Namely, a symmetrical cell with Ni/YSZ electrodes and a full cell with a Ni/GDC fuel electrode, shown in Fig. 1a and c, respectively. Their respective DRTs show in both cases a sensitivity to the quaternary variation only in the low frequency regime. In the case of Ni/YSZ the peak at approximately 25 Hz can be solely attributed to a concentration related process, while in the case of the used Ni/GDC electrode it is overlapping with thermally activated electrochemical surface reaction processes (see Figure S1 (ESI) for a temperature variation with both cells). A complete description of all peaks in the DRTs is not given at this point, the reader is forwarded to our earlier works, where comprehensive analyses of these cells have been performed [3,17,23]. The total polarization resistance of both cells is plotted over Λ_{diff} in Fig. 1e. The effective microstructure parameters of both cells obtained from the linear fit are in a similar range (781.7 m^{-1} vs. 626.6 m^{-1}) which arises from the fact that both cells have been tested in very similar setups and in electrolyte supported cells that are sufficiently porous, gas diffusion is dominated rather by the current collecting mesh than by the electrode pores. Effectively, these values can be projected to a gas diffusion resistance of 7.4 mΩ cm^2 (Ni/YSZ) and 9.2 mΩ cm^2 (Ni/GDC) of a single electrode at 800 °C and 5% steam in hydrogen.

Binary diffusion coefficients calculated by the Chapman-Enskog theory can exhibit uncertainties of up to around 10% compared to experimental studies [21], while additional deviations may arise from the application of the Wilke approximation. These uncertainties in D_i^{MC} introduce a systematic uncertainty in the calculated G_{eff}. However, as G_{eff} is obtained by fitting the model to the experimental impedance data, part of this uncertainty is compensated by the fitting procedure. Consequently, the impact of uncertainties in D_i^{MC} on the predicted diffusion resistance is expected to be limited, and the resulting values remain representative of the experimentally observed behavior.

3.1.2. Accessing G_{eff} via balancing H_2/H_2O with CO/CO_2

Alternatively, as earlier suggested by Mogensen et al., the diffusion resistance can be experimentally accessed by a change from a hydrogen/steam (H_2/H_2O) atmosphere to a carbon monoxide / carbon dioxide (CO / CO_2) atmosphere [12]. As long as the ratio between reduced components ($H_2 + CO$) to oxidized components ($H_2O + CO_2$) is kept constant, contributions from gas conversion will not change. It has to be noted, that when reformate mixtures of H_2, H_2O, CO and CO_2 are used, the equilibrium of the reverse water-gas shift reaction has to be considered and gases should be added already in their equilibrium composition, otherwise the concentration might vary to a non-negligible amount [23,24].

This alternative method is only applicable when a concentration impedance is visible as a distinct feature and can be extracted by a CNLS fit. Thus, it is not suitable for testing MIEC materials with large chemical capacitances, such as Ni/GDC. In the case of the Ni/YSZ electrode G_{eff} can be determined from the following relation, derived in our earlier study based on the assumption of two parallel gas diffusion resistances arising from the CO/CO_2 couple and the H_2/H_2O couple[23]:

$$R_{\text{LF}} = G_{\text{eff}}^{-1} \cdot \underbrace{\left(\frac{\widetilde{RT}}{2F}\right)^2 \left[\left(\frac{1}{D_{\text{CO}}^{\text{MC}} x_{\text{CO}}} + \frac{1}{D_{\text{CO}_2}^{\text{MC}} x_{\text{CO}_2}}\right)^{-1} + \left(\frac{1}{D_{\text{H}_2}^{\text{MC}} x_{\text{H}_2}} + \frac{1}{D_{\text{H}_2}^{\text{MC}} x_{\text{H}_2\text{O}}}\right)^{-1}\right]^{-1}}_{\Lambda_{\text{diff}}^{\text{ref}}} + C_{\text{Conv}}, \tag{8}$$

where R_{LF} is the resistance of the low frequency concentration feature

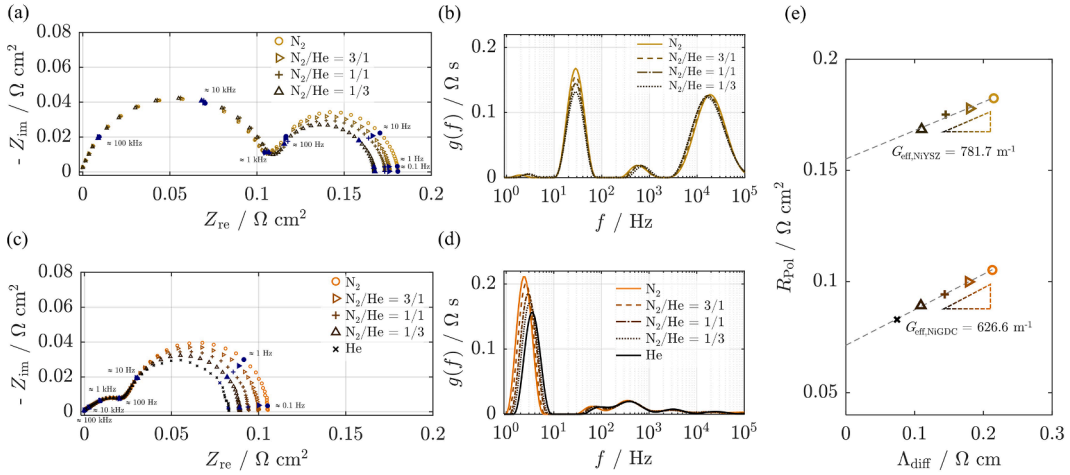

Fig. 1. **(a)** Series resistance corrected impedance spectra of one electrode (decadic steps marked in blue) and **(b)** corresponding DRT recorded during a quaternary inert gas variation on a symmetrical cell with Ni/YSZ electrodes. **(c)** Series resistance corrected impedance spectra and **(d)** corresponding DRT recorded during a quaternary variation on a full cell with a Ni/GDC fuel electrode. **(e)** Evaluation of polarization resistance of both cells over the effective gas diffusion term to access the effective microstructure parameter (symbols: data, lines: linear fit). $R^2_{\text{NiYSZ}} = 0.974$, $R^2_{\text{NiGDC}} = 0.999$. Conditions: $T_{\text{Ni/YSZ}} = 900$ °C; $T_{\text{Ni/GDC}} = 860$ °C; fuel electrode: 5% H_2O, 10% H_2, bal. N_2/He; air electrode (only (c) and (d)): 100% O_2.

and Λ_{diff}^{ref} the effective gas diffusion term of the reformate gas mixture. C_{conv} is then the remaining conversion contribution. In Fig. 2 the EIS measurements and calculated DRTs of eleven hydrogen to carbon ratios are shown. The ratio between oxidized species (H_2O and CO_2) and reduced species (H_2 and CO) is thereby kept constant at a value of 1 (exact concentrations see Table I). As a result of higher amounts of CO and CO_2 in the mixture, the high-frequency feature as well as the low-frequency feature are increasing in resistance. This is due to the slower kinetics of the electrochemical conversion of CO/CO_2 (high frequency feature) and slower diffusion of CO/CO_2 [23,24]. Note, that no distinct peak at low frequencies, associated with gas diffusion of the CO/CO_2-pair in coupling with the water-gas shift surface chemistry is observable, which is often referred to as P_{ref} [16,24]. This can be explained by the relatively low Ni surface area of the current collector mesh, compared to a porous Ni/YSZ substrate with which P_{ref} is usually observed [25,26].

The frequency separation between the features however, is still larger than two orders of magnitude, so the resistance of the low-frequency concentration feature R_{LF} can be straightforwardly extracted by a CNLS fit with a R-CPE element. When we now plot R_{LF} over Λ_{diff}^{ref} a straight line is obtained. A linear fit yields a G_{eff} of 706.5 m^{-1}, nearly identical to the one obtained by the quaternary variation with inert diluents presented earlier, confirming the validity of the alternative approach. The y-axis intercept equals to 3 mΩ cm^2, and is in this case the remaining gas conversion resistance inside the low frequency feature,

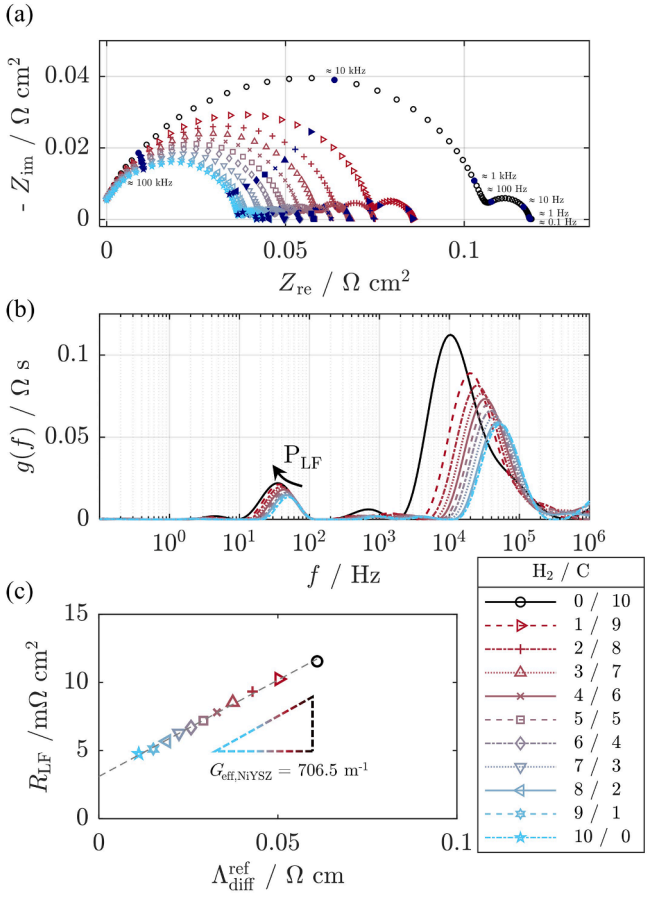

Fig. 2. **(a)** Series resistance corrected impedance spectra of one electrode (decadic steps marked in blue) and **(b)** corresponding DRT recorded during a stepwise change from a H_2/H_2O-atmosphere to a CO/CO_2-atmosphere on a symmetrical cell with Ni/YSZ electrodes. **(c)** Evaluation of low frequency resistance over the effective gas diffusion term of the reformate gas mixture to access the effective microstructure parameter (symbols: data, line: linear fit). $R^2 = 0.998$. Conditions: $T = 860$ °C; Set concentrations can be found in Table I.

Table I
Molar fractions of supplied gases set to acquire the spectra given in Fig. 2.

H_2 / C	x_{H_2} / -	x_{H_2O} / -	x_{CO} / -	x_{CO_2} / -
0 / 10	0.00	0.00	0.50	0.50
1 / 9	0.05	0.05	0.45	0.45
2 / 8	0.10	0.10	0.40	0.40
3 / 7	0.14	0.16	0.36	0.34
4 / 6	0.19	0.21	0.31	0.29
5 / 5	0.24	0.26	0.26	0.24
6 / 4	0.29	0.31	0.21	0.19
7 / 3	0.34	0.36	0.16	0.14
8 / 2	0.40	0.40	0.10	0.10
9 / 1	0.45	0.45	0.05	0.05
10 / 0	0.50	0.50	0.00	0.00

which is naturally minimized at a ratio between oxidized and reduced species of 1.

It must be noted, that the addition of CO and CO_2 poses the risk of introducing trace contaminants, commonly present in industrial CO and CO_2 gas bottles, such as sulfuric compounds in the ppb range, which cause a (usually reversible) degradation of the process associated with electrode activation [27,28]. Inhibition of the water-gas shift reaction by sulfur poisoning can also affect low-frequency resistance contributions [29]. However, such changes usually appear after a delay of several hours [30]. We therefore recommend to perform the measurement before significant changes of the resistance appear and afterwards regenerate in a carbon-free gas mixture. Recorded spectra should always be checked for symptoms of degradation, such as significant changes in capacitance due to a loss of active sites, high KK residuals or low-frequency drift. In the presented measurements, CNLS fits revealed no significant changes in capacitance due to introduction of CO/CO_2 in the high frequency part of the spectrum (228 μF cm^{-2} in H_2/H_2O vs. 250 μF cm^{-2} in CO/CO_2) and maximum KK residuals were 0.16%. However, in the case of the CO/CO_2 mixture, one can observe a slight low frequency drift which might indicate the onset of sulfur poisoning but can also be the result of a not yet fully stabilized cell. The effect is minimal but could explain the very slight difference of G_{eff} (781.7 m^{-1} vs. 706.5 m^{-1}) compared to the inert diluent variation.

3.2. Determination of the gas conversion resistance

Gas conversion resistances arise due to in-plane concentration differences between inlet and electrode surface in a situation where *convective* gas transport in the channel is determining the loss mechanism. Earlier studies have explored the mechanism and effect of conversion losses with numerical studies [31–33], experimental investigations [15,16,34–36] and some authors have derived analytical expressions for the conversion impedance under various test configurations [13,14,37]. These analytical expressions have been useful to confirm the presence of a gas conversion contribution by comparing the general trend to the prediction by the analytical expression. On the other hand, an exact match of experimental data and the idealized analytical equations is rare. As a consequence, we propose to introduce a conversion calibration factor k_{conv} according to the equation:

$$R_{conv}^{calib} = k_{conv} \cdot \frac{\widetilde{R}T}{F^2 J_{in}} \left(\frac{1}{x_{in,H_2O}} + \frac{1}{x_{in,H_2}} \right). \quad (9)$$

The equation is a slightly modified version of Eq. (4) and (5) and yields the CSTR model for $k_{conv} = 0.25$ and the PFR model for $k_{conv} = 0.125$. Most importantly, no *a-priori* decision must be taken whether CSTR and PFR model may be more suitable to describe the data and moreover, k_{conv} can account for linear deviations from the ideal models.

The factor k_{conv} can be obtained by a simple experiment: A variation of flow rate at OCV, constant temperature, concentration, and pressure. The measured resistances at each flow rate are then linearly fitted to an

equation in the form of:

$$R_{\text{meas}} = k_{\text{conv}} \cdot \underbrace{\frac{\widetilde{R}T}{F^2 J_{\text{in}}} \left(\frac{1}{x_{\text{in,H}_2\text{O}}} + \frac{1}{x_{\text{in,H}_2}} \right)}_{\Lambda_{\text{conv}}} + C_2, \tag{10}$$

where R_{meas} is the measured polarization resistance and C_2 the sum of the gas diffusion resistance and all thermally activated polarization resistance contributions. Alternatively, when a distinct concentration feature is visible and separately fitted, R_{meas} and C_2 correspond to the measured low-frequency resistance and the remaining gas diffusion contribution, respectively. Λ_{conv} denotes the effective gas conversion term. Note again, that the gas conversion resistance, similar to the gas diffusion resistance, approaches infinity for mixtures containing either only hydrogen or steam as electroactive compound. When performing this experiment, one should always select a sufficient amount of humidification.

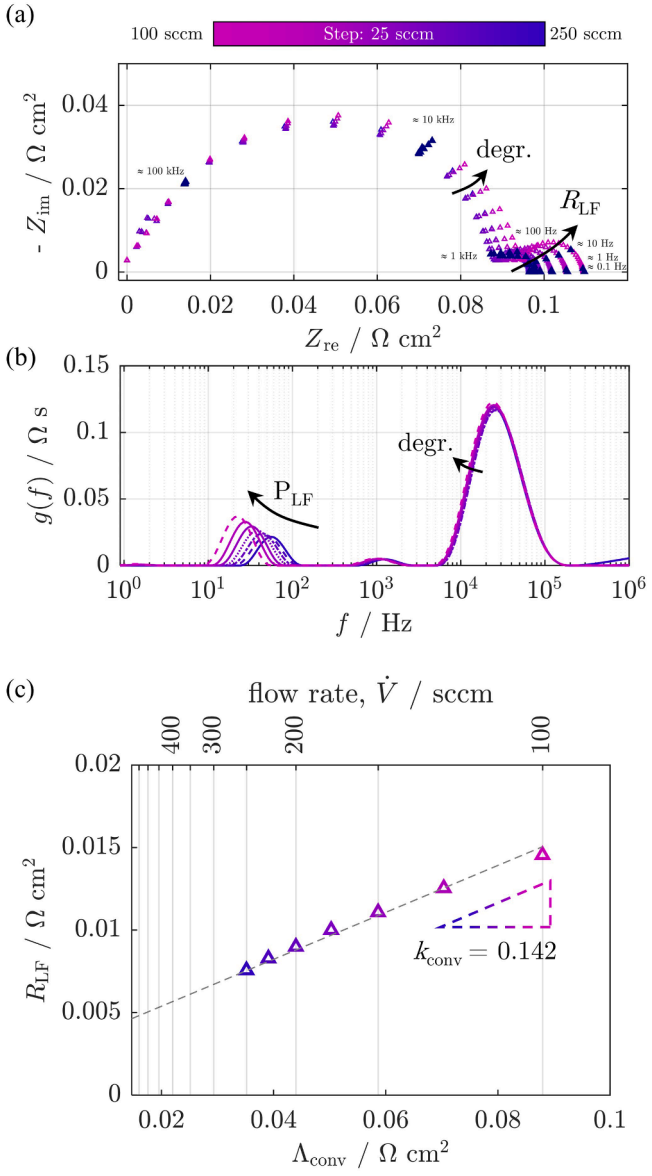

Fig. 3. **(a)** Series resistance corrected impedance spectra (decadic steps marked in blue) and **(b)** corresponding DRT recorded during a stepwise change of flow rate on a symmetrical cell with Ni/YSZ electrodes. (Spectrum of a single electrode is displayed) **(c)** Evaluation of low frequency resistance over the effective gas conversion term to access the conversion calibration factor (symbols: data, lines: linear fit). $R^2 = 0.987$. Conditions: $T = 900\,^{\circ}\text{C}$; 20% H_2O in H_2.

The method is demonstrated with the results shown in Fig. 3. A symmetrical cell with Ni/YSZ electrodes was used to perform a flow-rate variation between 100 sccm and 250 sccm per electrode under 20% H_2O (bal. H_2) and 900 °C. The results of the EIS measurements and corresponding DRTs are shown in Fig. 3a and b, respectively. Due to the decreasing flow rate, the low frequency feature increases in magnitude, as predicted by Eq. (9). Also, a slight non-reversible degradation was found in the high-frequency electrode activation term. Therefore, only the resistance from the low-frequency feature R_{LF} was used for the analysis. Degradation of the low-frequency contribution (i.e. change in gas conversion due to a complete loss of geometric cell area), which would negatively affect the determination k_{conv}, could be safely excluded as the low frequency peak appeared identical in a reference measurement before and after the flow-rate variation. The reason for the observed degradation of the high frequency term was not investigated, but is in a range (~0.1 mΩ cm^2 h^{-1}) that is not unusual for electrolyte supported Ni/YSZ electrodes fabricated in a laboratory environment. It is commonly attributed to a loss of active sites due to migration, coarsening and depletion of Ni particles [38].

In Fig. 3c, R_{LF} is plotted over Λ_{conv}, i.e. the inverse flow rate. The resistance shows a linear behavior over the inverse flow rate and by fitting Eq. (10) to the data a conversion calibration factor of 0.142 is obtained. The y-axis intercept C_2 obtained from the fit is 2.5 mΩ cm^2, which is precisely the value of the gas diffusion resistance obtained through the method described in the preceding section via Eq. (6).

In order to validate the presented method, a variation of the steam partial pressure between 5% up to 90% was performed with the same symmetrical cell with Ni/YSZ electrodes. The results can be seen in Fig. 4. EIS and DRT (Fig. 4a and b) reveal a decrease of the low frequency feature (P_{LF}) from 5% to 50% H_2O, followed by an increase of the feature up to 90% H_2O. The result of the CNLS-fit of the low frequency feature, confirms the parabolic nature of the concentration resistance R_{LF} (Fig. 4c). Also, we have plotted the prediction of the feature via 1) only the gas diffusion model (Eq. (6)), 2) addition of the gas diffusion model and the ideal CSTR model (Eq. (6) and (4)), 3) addition of the gas diffusion model and the ideal PFR model (Eq. (6) and (5)), and 4) the introduced conversion calibration method (Eq. (6) and (9)). The best agreement is observed with the conversion calibration method, as observed from the absolute errors in Fig. 4d.

The result of the conversion calibration ($k_{\text{conv}} = 0.142$) is close to the value of the ideal PFR model ($k_{\text{conv}} = 0.125$), therefore the ideal PFR model would also yield acceptable results. However, from the used setup ($A_{\text{cell}} = 1$ cm^2, $\dot{V}_{\text{in}} = 150$ sccm per electrode) the *a-priori* decision of a PFR model is not necessarily intuitive, as axial concentration gradients are expected to be small for the 1 cm channel considered here. The conversion calibration accounts for linear deviations from an ideal case, caused from the symmetrical setup (e.g. uneven flow distribution between both cell sides), the total channel width to cell area ratio and small bypasses caused by slightly erroneous positioning of the ceramic housing parts. The role of bypasses in particular, will be more thoroughly explained in the following section.

Notably, the method is not only applicable to the fuel electrode side, but can also be extended to the air electrode side. Necessary modifications to the equations and a validation of the applicability of the method can be found in Appendix A.

3.3. Calibrate non-idealities from the testing setup

The earlier shown method, based on the conversion calibration factor, can be used to quantify changes in the conversion resistance due to a non-ideal testing setup. We demonstrate this by performing a flow-rate variation with a setup where 1) the total flow passes over the electrode surface (“no bypass”) and 2) an additional bypass volume along the edges of the electrode is introduced (“bypass”). The realization of this

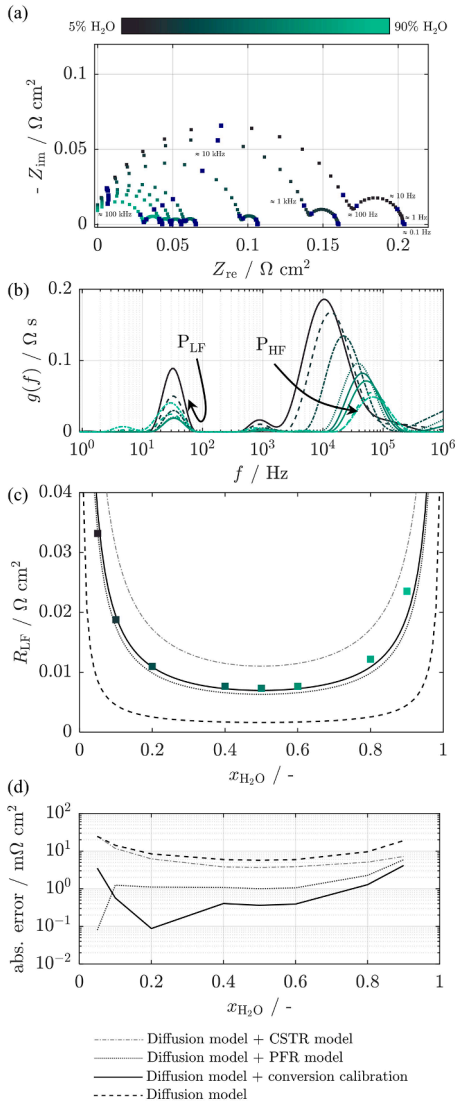

Fig. 4. **(a)** Series resistance corrected impedance spectra of one electrode (decadic steps marked in blue) and **(b)** corresponding DRT recorded during a stepwise change of H_2O concentration on a symmetrical cell with Ni/YSZ electrodes. **(c)** Evaluation of the low frequency resistance over steam concentration and comparison to the discussed model approaches (symbols: data, lines: model predictions). **(d)** Absolute prediction error of the discussed model approaches. The diffusion model combined with a calibrated conversion resistance yield the most accurate prediction of the concentration resistance in a wide steam concentration range. Conditions: $T = 900\,°C$, 150 sccm per electrode. Ohmic resistances were excluded to allow a better comparison of polarization resistances.

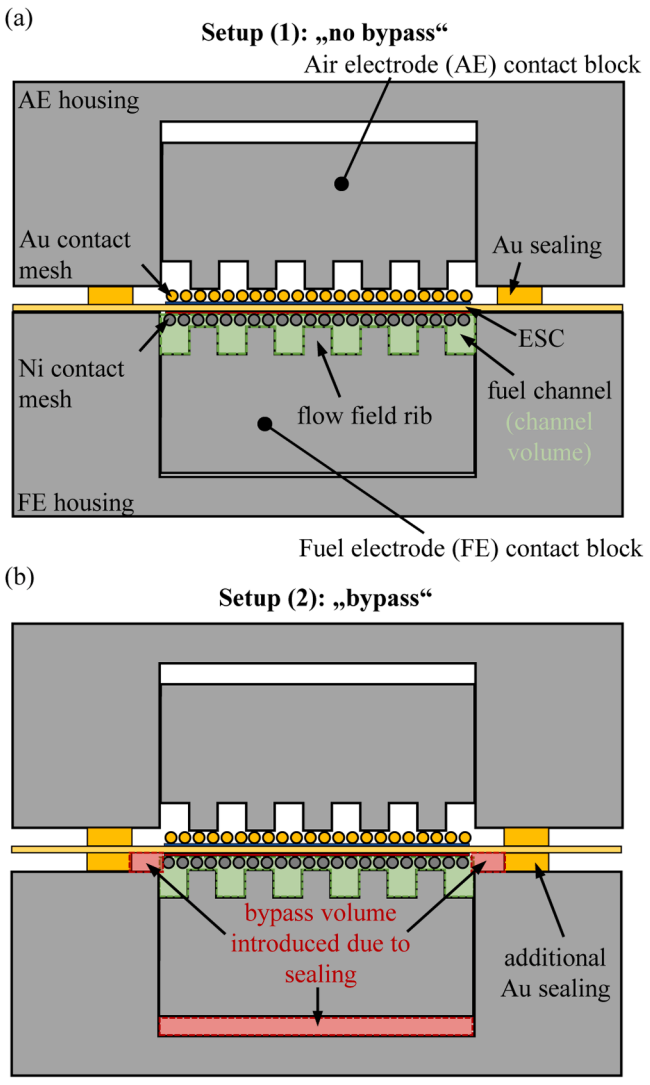

Fig. 5. Schematic of the cell housing in cross-section view with **(a)** no bypass at the fuel side and **(b)** an introduced bypass due to an additional sealing ring.

experiment is shown in Fig. 5. Setup 1) is the common configuration used for testing small scale SOCs in our group [18] (Fig. 5a). Setup 2 is realized with an additional gold (Au) sealing on the fuel side, between electrolyte and housing. The introduced bypass volume is marked in red in Fig. 5b.

The cell used for the test comprised a 1 cm^2 Ni/GDC fuel electrode and a GDC/LSCF air electrode on a 3YSZ electrolyte support. The air electrode was supplied with pure oxygen to exclude concentration effects on the air side. Both setups were tested with the same, identical cell. At first, the test was performed with setup 2) ("bypass"), then cooled down and re-heated under safety gas with setup 1) ("no bypass"). In this way, we can make sure that the electrode properties are similar in both tests.

The results of the flow-rate variation with both setups are displayed in Fig. 6. The impedance spectra reveal a change in the low-frequency regime, where the "bypass setup" shows a higher sensitivity to flow rate, than the "no bypass setup". The DRT shows, that processes up to 100 Hz are affected, which demonstrates that frequencies affected by gas conversion span up to four decades.

Another interesting observation is that at flow rates < 100 sccm (bypass) or < 90 sccm (no bypass) an additional peak (P_{conv}) appears at 0.3 Hz. Geisler et al. have observed a similar low frequency semicircle with a 1 cm^2 anode supported SOFC, sensitive to flow rate and appearing at flow rates < 100 sccm [39]. They assigned the conversion resistance solely to this semicircle, concluding conversion resistances would be neglectable at flow rates > 100 sccm cm^{-2}. However, the presented experiment demonstrates that the frequency range of the conversion resistance is not limited to a single peak or semicircle, but can overlap with multiple processes in a frequency range between 0.1 Hz up to 100 Hz and even at 250 sccm cm^{-2} it is not necessarily neglectable. Yet, it has to be noted that the experiments by Geisler et al. were performed with a cell comprising a thick anode support (~1.5 mm), so in their work the gas conversion resistance might be significantly smaller than the resistance from gas diffusion through the porous support. Thus, their assumption of a neglectable gas conversion at flow rates > 100 sccm cm^{-2} might still be valid, as gas diffusion strongly dominates the low frequency response in their work. In this work however, an ESC is

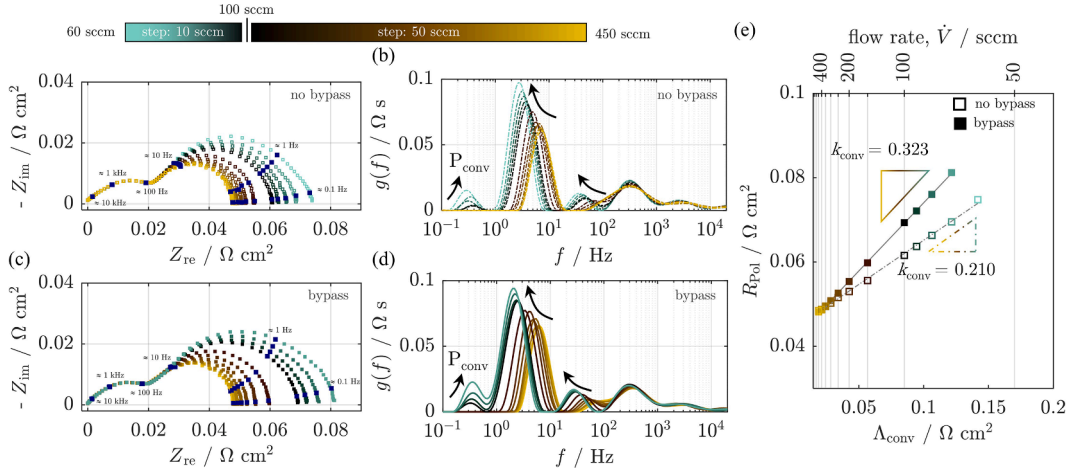

Fig. 6. **(a)** Series resistance corrected impedance spectra (decadic steps marked in blue) and **(b)** corresponding DRT recorded during a stepwise change of flow rate on the fuel side of a full cell with Ni/GDC fuel electrode with no bypass present and **(c)** + **(d)** with a bypass introduced to the housing setup. **(e)** Evaluation of polarization resistance over the effective gas conversion term to access the conversion calibration factor (symbols: data, lines: linear fit). $R^2_{\text{nobypass}} = 0.998$, $R^2_{\text{bypass}} = 0.999$. Conditions: $T = 860\,°\text{C}$; fuel electrode: 20% H_2O, bal. H_2; air electrode: 100% O_2. Ohmic resistances were excluded to allow a better comparison of polarization resistances.

employed, where much smaller gas diffusion contributions are present.

The evaluation of polarization resistance over the effective gas conversion term Λ_{conv} is displayed in Fig. 6e. From the bypass setup, a steeper slope and thus a higher k_{conv} is obtained than in the setup without bypass (0.323 vs. 0.210). This results from the fact that the effective volume that interacts with the electrode is smaller with the bypass present, which causes a larger conversion resistance. The magnitude of the resistance increase is precisely quantified by k_{conv}, which enables a reliable estimation of the gas conversion resistance at arbitrary inlet flow rates and steam (or hydrogen) partial pressures (see Appendix B). Since the time constant of the total concentration resistance overlaps with the thermally activated porous electrode response, the validation of the approach is not straightforward with a Ni/GDC electrode. This challenge is tackled in the next chapter, by comparing the activation energies of the polarization resistances obtained with both setups.

3.4. Accessing the activation energies from MIEC electrodes with large chemical capacitances

In MIEC-containing electrodes with large chemical capacitances the time constants of the electrochemical porous electrode response may appear to be very close to the time constant of the concentration impedance [3–8]. When the electrode performance is high, the resulting Arrhenius plot of the fitted resistance will not appear as a straight line but flattens towards higher temperatures due to the weak temperature dependency of concentration losses [9,10]. In order to avoid underestimation of the activation energy, the total resistance must be adequately corrected by the total gas concentration term.

To demonstrate the described issue, we have performed a temperature variation between 630 °C and 890 °C with the "bypass" setup and the "no bypass" setup under 5% steam, balanced in hydrogen and with a flow rate at the fuel electrode of 250 sccm. A wide temperature range of at least 200 K is hereby essential to visualize the apparent curvature of the Arrhenius plot.

The Arrhenius plots of both setups, with and without concentration correction, can be seen in Fig. 7. Evidently, without correction, the plots do not appear as a straight line but a curvature is visible which causes a flattening towards higher temperatures. The curvature is stronger expressed with the "bypass" setup, which also lowers the obtained apparent activation energy (0.78 eV). The activation energy of the "no bypass" setup is higher (0.93 eV) but still an effect of the curvature is visible.

However, with the correction by gas diffusion and conversion applied, the Arrhenius plot obtained in both setups turned linear. Also, both setups result in a nearly identical activation energy (1.07 eV vs. 1.1 eV) of the polarization resistance.

As in both setups the same, identical cell was used, this is a successful validation of the resistance correction approach to extract the intrinsic activation energy of a high-capacitance-MIEC containing cell. In contrast, the assumption of ideal PFR behavior would result in an activation energy of 0.9 eV and the assumption of ideal CSTR behavior to 0.99 eV (both not shown in the figure), which underlines the necessity of the conversion calibration method.

The correction also reveals a small degradation of the intrinsic polarization resistance after the thermal cycle, which was quantified as 8.5% at the chosen reference point (830 °C, 5% H_2 in H_2O). As the polarization resistance is arising from a sum of air- and fuel electrode processes which may be unequally affected by the thermal cycle, the activation energy of the total polarization resistance could have been altered, complicating a direct comparison. Nevertheless, the very similar activation energies obtained indicate that a significant effect of ageing on the activation energy can be safely excluded. However, this might potentially explain the very slight deviation of 0.03 eV obtained in the analysis.

4. Discussion

A summary of determined effective microstructure parameters (G_{eff}) and conversion calibration factors (k_{conv}) is given in Table II. Additionally, we compare the effective microstructure parameters obtained using only the boundary points of the quaternary gas variation, which corresponds to the method proposed by Grosselindemann et al. [3]. The comparison confirms that the resulting values are nearly identical, implying that, in principle, only two measurements are sufficient to determine G_{eff}. However, using multiple measurements to determine the slope makes it easier to identify outliers or experimental drift, thereby increasing the reliability of the parameter determination.

Notably, measurements with Ni/GDC electrodes revealed lower G_{eff} values compared to Ni/YSZ electrodes. This might indicate that slight

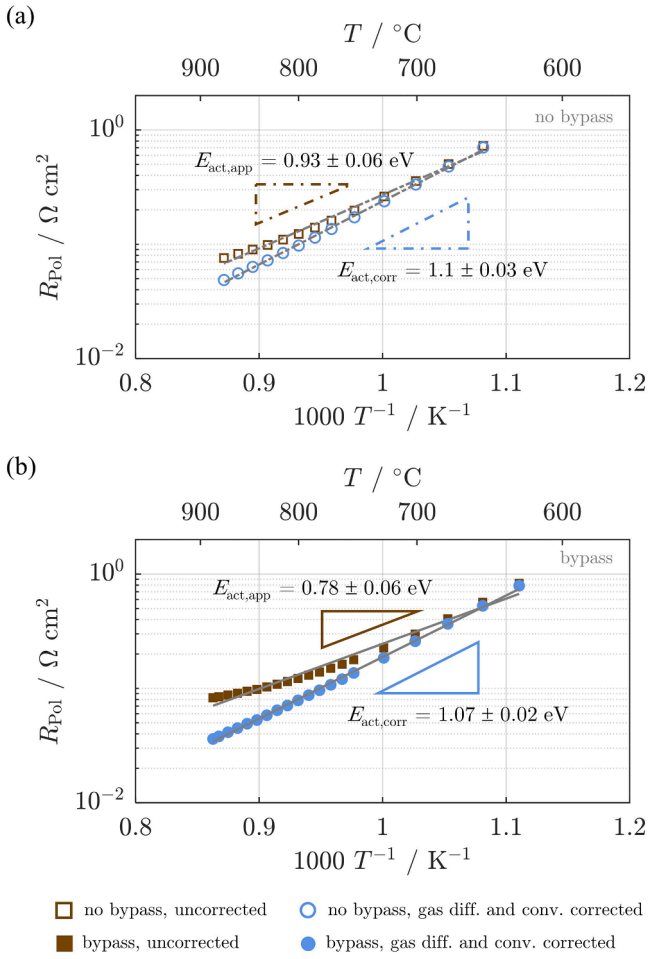

Fig. 7. (a) Arrhenius graph obtained from a temperature variation with no bypass present (R^2_{app}= 0.991, R^2_{corr}= 0.999) and **(b)** with a bypass introduced to the housing setup (R^2_{app}= 0.977, R^2_{corr}= 0.999), with and without correction by concentration resistance contributions (symbols: data, lines: linear fit) of a cell containing a Ni/GDC fuel electrode. The correction reveals nearly identical intrinsic activation energies with both setups, confirming an activation energy of around 1.1 eV and validating the presented approach for correcting concentration resistance contributions. Conditions: fuel electrode: 5% H_2O, bal. H_2 (250 sccm); air electrode: 100% O_2.

differences in electrode microstructure affect the determination of G_{eff}, suggesting that the assumption of negligible pore diffusion resistance originating from the electrode functional layer [3,10] is not fully valid. However, the obtained G_{eff} values for Ni/GDC and Ni/YSZ result in only a minor difference in the calculated gas diffusion resistance of <2 mΩ cm^2 (single electrode, 800 °C, 5% steam in hydrogen), which is within the measurement accuracy of the potentiostat.

If helium is not available at the testing rig, G_{eff} can alternatively be determined by successive exchange of H_2 / H_2O with CO / CO_2, respectively. However, several aspects must be carefully considered:

- A distinct gas transport resistance-related feature must be visible, which can be clearly identified by its insensitivity to temperature variations.
- The gas mixture must be introduced already in equilibrium; otherwise, large concentration gradients may develop along the channel length. Within the equilibrium calculation, the formation of solid carbon due to the Boudouard reaction must also be reliably ruled out.
- Sulfur-containing species might be introduced as contaminants within the CO/CO_2 mixture, so the measurement should be performed before the onset of sulfur-induced passivation.

The results show a very similar G_{eff} value obtained from the H_2/H_2O vs. CO/CO_2 variation compared to the N_2 vs. He variation, which confirms the validity of the method. In principle, the approach can be further simplified by considering only the boundary points, i.e., by calculating the resistance difference between a binary H_2/H_2O mixture and a binary CO/CO_2 mixture. This approach again results in a very similar G_{eff} value while significantly reducing the experimental complexity. Moreover, binary diffusion coefficients are readily available, whereas the calculation of quaternary diffusion coefficients introduces additional sources of uncertainty. However, if the experimental setup allows for the supply of quaternary mixtures, we still recommend performing the full quaternary variation to minimize the risk of outliers affecting the determined value.

We argue that simply fitting the low-frequency feature with a single RQ element (or Warburg element) and assuming that it is solely composed of a gas diffusion resistance is insufficient and may lead to an overestimation of the diffusion resistance, as the feature can contain significant contributions from gas conversion resistance. The conversion calibration factor k_{conv} enables the quantification of linear deviations from the ideal PFR or CSTR behavior, which were previously developed to analytically describe the gas conversion resistance.

The range of k_{conv} values determined for different setups, summarized in Table II, demonstrates that even in highly optimized and idealized experimental arrangements, the assumption of ideal CSTR or PFR behavior can result in inaccurate predictions of the gas conversion resistance. Quantitatively, the assumption of ideal CSTR behavior leads to an absolute deviation in the predicted conversion resistance of 12 mΩ cm^2, 8 mΩ cm^2 and 4 mΩ cm^2 in the Ni/YSZ symmetric setup, the Ni/GDC full cell setup with bypass, and the Ni/GDC full-cell setup without bypass, respectively. Conversely, the assumption of PFR behavior results in prediction errors of 2 mΩ cm^2, 22 mΩ cm^2 and 9 mΩ cm^2. (calculated at 800 °C, 5% steam in hydrogen, single electrode, 250 sccm cm^{-2}).

Although some of these deviations are sufficiently small to suggest that high prediction accuracy could be achieved using idealized models, the appropriate reactor model cannot be determined *a priori*. All three measurements were performed using the same flow-field geometry, flow rate, and geometric electrode area, yet the best analytical prediction was obtained using either the PFR model (Ni/YSZ symmetric setup) or the CSTR model (Ni/GDC full cell without bypass). Therefore, it is advantageous to directly calibrate the gas conversion resistance for the specific experimental setup rather than relying on assumptions regarding the idealized flow behavior.

Furthermore, the method should not be applied to predict gas conversion resistance outside the calibrated flow-rate range, as a significant reduction in flow rate may induce a transition from PFR to CSTR behavior or vice versa [37]. In principle, such a transition could be identified in the calibration plot by a change in slope at low flow rates by a factor of two. However, all k_{conv} calibrations performed in this work were based on linear fits with (R^2) values above 0.98, confirming linear behavior over the entire investigated flow-rate range.

Finally, we note that, only in the case of a clearly distinguishable low-frequency feature associated with gas transport, the sole determination of G_{eff} using the methods presented here can be sufficient for a complete deconvolution. The gas conversion resistance can then simply be obtained from the difference between the total gas concentration resistance represented by the concentration-related feature and the calculated gas diffusion resistance (or the gas conversion resistance, if determined instead). Otherwise, if the gas concentration-related feature is not clearly separated, for example due to a high chemical capacitance of the electrode, the additional flow-rate variation is a definite requirement for a complete deconvolution.

Table II
Summary of determined parameters and their 95% confidence intervals in the corresponding configurations. Entries including "only boundary points" refer to a determination with the method according to Grosselindemann et al. [3].

Parameter	Electrode	Configuration	Variation	value	95% CI	Figure #
G_{eff}	Ni/YSZ	*sym.*	N_2 vs. He	781.7 m^{-1}	697.6 m^{-1} –889.1 m^{-1}	Fig. 1
	Ni/YSZ	*sym.*	N_2 vs. He (only boundary points)	749.4 m^{-1}	-	-
	Ni/GDC	full	N_2 vs. He	626.6 m^{-1}	614.0 m^{-1} – 639.8 m^{-1}	Fig. 1
	Ni/GDC	full	N_2 vs. He (only boundary points)	621.6 m^{-1}	-	-
	Ni/YSZ	*sym.*	H_2/H_2O vs. CO/CO_2	706.5 m^{-1}	694.3 m^{-1} – 719.1 m^{-1}	Fig. 2
	Ni/YSZ	*sym.*	H_2/H_2O vs. CO/CO_2 (only boundary points)	734.3 m^{-1}	-	-
k_{conv}	Ni/YSZ	*sym.*	flow rate	0.142	0.137 – 0.147	Fig. 3
	Ni/GDC	full (bypass)	flow rate	0.323	0.321 – 0.325	Fig. 6
	Ni/GDC	full (no bypass)	flow rate	0.210	0.206 – 0.214	Fig. 6

5. Conclusions

In this work, we aimed to offer a complete experimental design to fully deconvolute concentration (gas diffusion and conversion) losses in small-scale single SOC fuel electrodes. In a first step, we showed how an already existing approach [3] to deconvolute gas diffusion resistances can be extended to increase reliability. The extended approach relies on a stepwise variation of inert diluent ratio (N_2/He ratio) and can extract an effective microstructure parameter that can be used to predict the gas diffusion resistance at arbitrary operation points. Moreover, an alternative approach to access the same quantity is presented via a variation including a stepwise change from an H_2/H_2O atmosphere, towards a CO/CO_2 atmosphere, which gives access to the same effective microstructure parameter.

As a significant extension to earlier works, we have developed a method to precisely quantify contributions from gas conversion, based on a flow-rate variation. The novel gas diffusion and conversion prediction methods aligns perfectly with total measured concentration impedances over a wide concentration range. We have shown that the novel conversion calibration method predicts the conversion resistance with higher accuracy than the existing analytical CSTR and PFR approaches.

Ultimately, the approach is demonstrated with two experimental setups, one erroneous setup with a bypass present, the other with no bypass present. A cell with a high-capacitance fuel electrode (Ni/GDC) was used, so that concentration losses fully overlap with thermally activated losses, which causes a flattening of the Arrhenius graph at high temperatures. The flow-rate variation revealed higher conversion losses in the setup with the bypass present, which explained a stronger flattening of the Arrhenius graph towards high temperatures than without the bypass. However, the initially presented correction by diffusion and concentration losses enabled a correct extraction of the intrinsic activation energy of a high-capacitance MIEC containing cell, regardless of the setup employed.

CRediT authorship contribution statement

D. Esau: Conceptualization, Data curation, Formal analysis, Investigation, Methodology, Validation, Visualization, Writing – original draft. **D. Ewald:** Data curation, Formal analysis, Investigation, Writing – review & editing. **C. Grosselindemann:** Conceptualization, Methodology, Writing – review & editing. **A. Weber:** Funding acquisition, Project administration, Resources, Supervision, Writing – review & editing.

Declaration of competing interest

The authors declare that they have no known competing financial interests or personal relationships that could have appeared to influence the work reported in this paper.

Acknowledgments

The authors gratefully acknowledge funding from the Federal Ministry of Research, Technology and Space in the project H2Giga-HTEL-Stacks (BMBF 03HY124C) as well as European Union's Horizon Europe research and innovation program in the project FlyECO under grant agreement No 101138488 and by the UK Research and Innovation (UKRI) funding guarantee under the project reference 10106893. Views and opinions expressed are however those of the author(s) only and do not necessarily reflect those of the European Union, UKRI or CINEA. Neither the European Union nor the granting authorities can be held responsible for them. Sincere thanks are given to Sunfire SE, Kerafol GmbH & Co. KG and Elcogen AS for producing the test cells.

Supplementary materials

Supplementary material associated with this article can be found, in the online version, at doi:10.1016/j.electacta.2026.149566.

Appendix A

The equivalent approach can be straightforwardly transferred to deconvolute concentration losses from the air electrode side. Gas diffusion losses can be extracted via a change of inert diluent and the help of the following equation [11,40]:

$$R_{\mathrm{LF}}^{\mathrm{AE}} = G_{\mathrm{eff,AE}}^{-1} \cdot \underbrace{\left[\left(\frac{\widetilde{R}T}{2F}\right)^2 \frac{1}{D_{\mathrm{O_2}}^{\mathrm{MC}}} \left(\frac{1}{x_{\mathrm{O_2}}} - 1\right) \frac{1}{P}\right]}_{\Lambda_{\mathrm{diff}}^{\mathrm{AE}}} + C_{1,\mathrm{AE}}. \tag{A–1}$$

Thereby, $D_{\mathrm{O_2}}^{\mathrm{MC}}$ denotes the multicomponent diffusivity of oxygen in the inert diluent mixture. Depending on the thickness and pore size of the air electrode it is either the molar diffusion coefficient or an effective diffusion coefficient affected by Knudsen and molecular diffusion, usually calculatable via the Bosanquet approach [41]. In the present case, only molecular diffusion was considered as the air electrode (~24 µm) is significantly thinner than the current collector mesh (~250 µm) placed upon the electrode. Applying equation (A–1) to a change of inert diluent at the air electrode side, a $G_{\mathrm{eff,AE}}$ of 782 m^{-1} is obtained. Furthermore, contributions from gas conversion at the air electrode side can be described via [13]:

$$R_{\mathrm{Conv}}^{\mathrm{AE}} = k_{\mathrm{Conv}}^{\mathrm{AE}} \frac{\widetilde{R}T}{F^2 J_{\mathrm{in}}} \left(\frac{1 - x_{\mathrm{in,O_2}}^{\mathrm{AE}}}{x_{\mathrm{in,O_2}}^{\mathrm{AE}}}\right). \tag{A–2}$$

A linear fit of the low frequency resistance arising from air electrode side concentration losses to the equation

$$R_{\mathrm{Conv}}^{\mathrm{AE}} = k_{\mathrm{Conv}}^{\mathrm{AE}} \frac{\widetilde{R}T}{F^2 J_{\mathrm{in}}} \left(\frac{1 - x_{\mathrm{in,O_2}}^{\mathrm{AE}}}{x_{\mathrm{in,O_2}}^{\mathrm{AE}}}\right) + C_{2,\mathrm{AE}} \tag{A-3}$$

yields a conversion calibration factor $k_{\mathrm{conv}}^{\mathrm{AE}}$ of 0.088 (see Fig. A–1a). As observable in Fig. A–1b, the addition of the calibrated diffusion and conversion terms can accurately describe the low-frequency feature arising from air electrode concentration losses at oxygen contents < 21%.

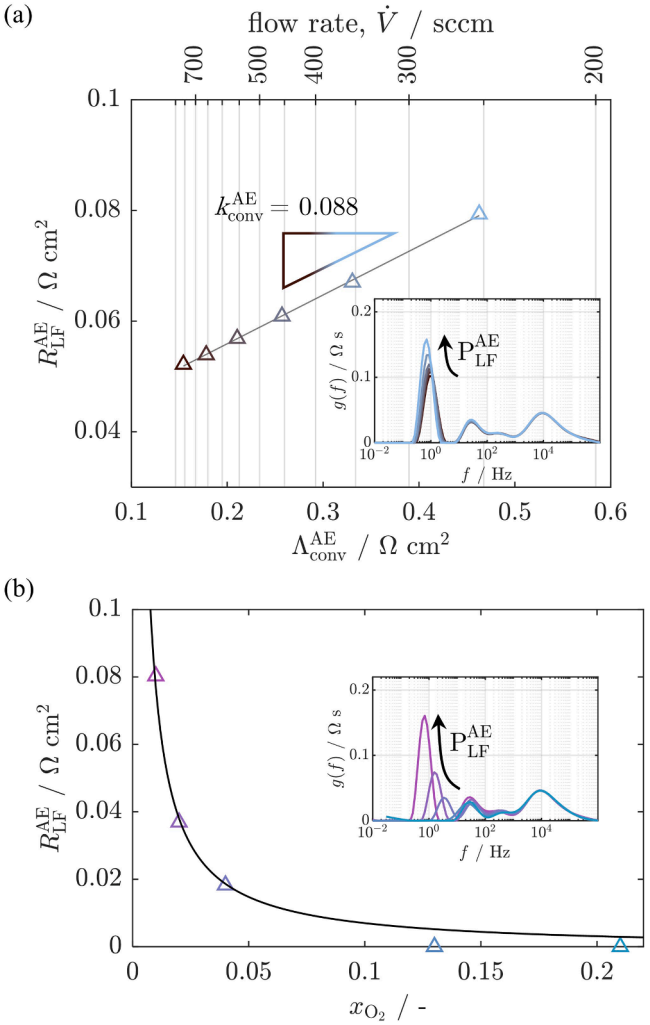

Fig. A–1. (a) Evaluation of low frequency air electrode concentration resistance over the effective gas conversion term to access the conversion calibration factor at the air side (symbols: data, line: linear fit). **(b)** Evaluation of the low frequency air electrode concentration resistance over oxygen concentration and comparison to the prediction by the summation of calibrated gas diffusion and gas conversion terms (symbols: data, line: model prediction). Conditions: $T = 700\,^{\circ}\mathrm{C}$. Fuel electrode side: 50% H_2O (bal. H_2). Air electrode side (only (a)): 1% O_2 (bal. N_2).

Appendix B

The derived conversion calibration factor can be used to estimate the conversion resistance at – in principle – arbitrary flow rates per cell area values. We have simulated the gas conversion resistance on the fuel side in our standardized setup ("no bypass") in the range between 10 and 1000 sccm cm^{-2} and steam (or hydrogen) contents between 50–100% (see Fig. B-1). The simulation reveals a steep increase in resistance for steam (or hydrogen) contents < 5% for all flow rates. Negligible gas conversion resistances (< 5 mΩ cm^{-2}) over a wide steam (or hydrogen) partial pressure range would require flow rates larger than 500 sccm cm^{-2}, which are rarely realized. However, it has to be noted that the actual magnitude of the gas conversion resistance is always a function of the present setup and the conversion calibration factor is only valid in a limited operation range, as a large change of flow rate, cell area or channel geometry can cause a change from a CSTR to a PFR situation, or vice versa.

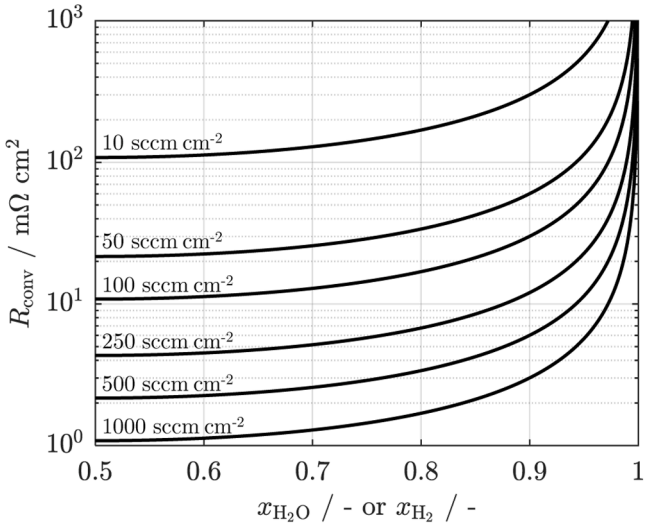

Fig. B–1. Simulation of the gas conversion resistance in the "no bypass" setup (k_{Conv} = 0.210) at flow rates from 10 to 1000 sccm cm^{-2} and from steam (or hydrogen) contents from 0.5 to 1. Due to the symmetry of Eq. (9), the x-axis range is limited from 0.5 to 1. OCV; T = 800 °C.

Data availability

Data can be found under the DOI: 10.35097/8vzhndvkb5443va7.

References

[1] W.G. Bessler, M. Vogler, H. Störmer, D. Gerthsen, A. Utz, A. Weber, E. Ivers-Tiffée, Phys. Chem. Chem. Phys. 12 (2010) 13888.
[2] W.G. Bessler, J. Warnatz, D.G. Goodwin, Solid State Ion. 177 (2007) 3371–3383.
[3] C. Grosselindemann, N. Russner, S. Dierickx, F. Wankmüller, A. Weber, J. Electrochem. Soc. 168 (2021) 124506.
[4] A. Hagen, A.K. Padinjarethil, J. Heijne, Electrochim. Acta 461 (2023) 142672.
[5] T. Nakamura, T. Kobayashi, K. Yashiro, A. Kaimai, T. Otake, K. Sato, J. Mizusaki, T. Kawada, J. Electrochem. Soc. 155 (2008) B563.
[6] A. Nenning, C. Bischof, J. Fleig, M. Bram, A.K. Opitz, Energies 13 (2020) 987.
[7] V.A. Rojek-Wöckner, A.K. Opitz, M. Brandner, J. Mathé, M. Bram, J. Power Sources 328 (2016) 65–74.
[8] A. Nenning, L. Volgger, E. Miller, L.V. Mogni, S. Barnett, J. Fleig, J. Electrochem. Soc. 164 (2017) F364–F371.
[9] A. Nenning, M. Holzmann, J. Fleig, A.K. Opitz, Mater. Adv. 2 (2021) 5422–5431.
[10] M. Riegraf, R. Costa, G. Schiller, K.A. Friedrich, S. Dierickx, A. Weber, J. Electrochem. Soc. 166 (2019) F865–F872.
[11] S. Primdahl, M. Mogensen, J. Electrochem. Soc. 146 (1999) 2827–2833.
[12] M.B. Mogensen, S.D. Ebbesen, S.H. Jensen, X. Sun, A. Hauch, M. Chen, ECS Trans. 78 (2017) 2133–2139.
[13] S. Primdahl, M. Mogensen, J. Electrochem. Soc. 145 (1998) 2431–2438.
[14] S.H. Jensen, A. Hauch, P.V. Hendriksen, M. Mogensen, J. Electrochem. Soc. 156 (2009) B757.
[15] S.D. Ebbesen, X. Sun, M.B. Mogensen, Faraday Discuss. 182 (2015) 393–422.
[16] J.-C. Njodzefon, C.R. Graves, M.B. Mogensen, A. Weber, J. Hjelm, J. Electrochem. Soc. 163 (2016) F1451–F1462.
[17] V. Sonn, A. Leonide, E. Ivers-Tiffée, J. Electrochem. Soc. 155 (2008) B675.
[18] D. Klotz, A. Weber, E. Ivers-Tiffée, Electrochim. Acta 227 (2017) 110–126.
[19] M. Schönleber, D. Klotz, E. Ivers-Tiffée, Electrochim. Acta 131 (2014) 20–27.
[20] E.L. Cussler, Diffusion: Mass Transfer in Fluid Systems, Cambridge university press, 2009.
[21] B.E. Poling, J.M. Prausnitz, O.C.J. Paul, R.C. Reid, The Properties of Gases and Liquids, Mcgraw-hill New York, 2001.
[22] D.F. Fairbanks, C.R. Wilke, Ind. Eng. Chem. 42 (1950) 471–475.
[23] D. Esau, C. Grosselindemann, S. Sckuhr, F. Kullmann, A. Lindner, Z. Liang, F. Fuchs, A. Weber, J. Electrochem. Soc. 171 (2024) 054522.
[24] A. Kromp, A. Leonide, A. Weber, E. Ivers-Tiffée, J. Electrochem. Soc. 158 (2011) B980.
[25] H. Zhu, A. Kromp, A. Leonide, E. Ivers-Tiffée, O. Deutschmann, R.J. Kee, J. Electrochem. Soc. 159 (2012) F255–F266.
[26] Y. Liu, Z. Lyu, M. Han, L. Ma, Electrochim. Acta 544 (2025) 147647.
[27] D. Esau, S. Horlick, C.-Y. Tsai, A. Weber, J. Power Sources 659 (2025) 238429.
[28] M. Riegraf, K. Develos-Bagarinao, I. Biswas, R. Costa, J. Power Sources 559 (2023) 232669.
[29] A. Kromp, S. Dierickx, A. Leonide, A. Weber, E. Ivers-Tiffée, J. Electrochem. Soc. 159 (2012) B597–B601.
[30] A. Weber, S. Dierickx, A. Kromp, E. Ivers-Tiffée, Fuel Cells 13 (2013) 487–493.
[31] W.G. Bessler, S. Gewies, J. Electrochem. Soc. 154 (2007) B548.
[32] J. Taubmann, X. Sun, O.B. Rizvandi, H.L. Frandsen, J. Power Sources 588 (2023) 233739.
[33] K. Takano, S. Nagata, K. Nozaki, A. Monma, T. Kato, Y. Kaga, A. Negishi, K. Kato, T. Inagaki, H. Yoshida, J. Power Sources 132 (2004) 42–51.
[34] B. Liu, H. Muroyama, T. Matsui, K. Tomida, T. Kabata, K. Eguchi, J. Electrochem. Soc. 158 (2011) B215.
[35] T. Kato, K. Nozaki, A. Negishi, K. Kato, A. Monma, Y. Kaga, S. Nagata, K. Takano, T. Inagaki, H. Yoshida, J. Power Sources 133 (2004) 169–174.
[36] A. Momma, Y. Kaga, K. Takano, K. Nozaki, A. Negishi, K. Kato, T. Kato, T. Inagaki, H. Yoshida, K. Hosoi, Solid State Ion. 174 (2004) 87–95.
[37] T. Jacobsen, P.V. Hendriksen, S. Koch, Electrochim. Acta 53 (2008) 7500–7508.
[38] M.S. Khan, S.-B. Lee, R.-H. Song, J.-W. Lee, T.-H. Lim, S.-J. Park, Ceram. Int. 42 (2016) 35–48.
[39] H. Geisler, A. Kromp, S. Hirn, A. Weber, E. Ivers-Tiffée, ECS Trans. 57 (2013) 2691–2704.
[40] A. Leonide, Y. Apel, E. Ivers-Tiffee, ECS Trans. 19 (2009) 81–109.
[41] R.B. Bird, W.E. Stewart, E.N. Lightfoot, Transport Phenomena, Wiley, 2009.